Upper mantle structure of southern Africa from Rayleigh wave tomography

Aibing Li[1] and Kevin Burke[1]

Received 1 February 2006; revised 9 May 2006; accepted 14 June 2006; published 10 October 2006.

[1] Rayleigh wave phase velocities in southern Africa have been obtained at 18 periods from 20 to 167 s using a two-plane wave method. These phase velocities are utilized in subsequent inversions to solve for shear wave structure in the crust and upper mantle of southern Africa. A fast lithosphere lid is imaged beneath most parts of southern Africa. The lid thickness is estimated on the basis of the variation of shear wave velocity with depth and ranges from ~80 km beneath the Namaqua-Natal belt to 180 ± 20 km beneath the Kaapvaal craton. Relative low velocities are observed under the Cape Fold Belt and beneath the tectonic border regions in the shallow upper mantle. The Bushveld Complex is relatively slower than its surroundings above 100 km, probably because of high iron content that resulted from an intracratonic intrusion at 2.05 Ga. A relative low-velocity zone (LVZ) is observed at the depths of 160–260 km across southern Africa with an average velocity of ~4.5 km/s. This layer, although not absolutely slow, is ~4% slower than the fast lithosphere above it. The velocity reduction in this layer varies from 4.8% at the edges of the Kaapvaal craton to 1.5% at its center. Such a large velocity reduction and a strong lateral variation in the LVZ cannot be totally attributed to compositional and petrologic effects. Our preferred interpretation is that the LVZ is largely caused by high temperature. It is probably associated with sublithospheric mantle convection and should make contributions to supporting the high elevation of southern Africa.

Citation: Li, A., and K. Burke (2006), Upper mantle structure of southern Africa from Rayleigh wave tomography, *J. Geophys. Res.*, *111*, B10303, doi:10.1029/2006JB004321.

1. Introduction

[2] Southern Africa contains two of the oldest continental blocks on Earth, the Kaapvaal and Zimbabwe cratons. The Kaapvaal craton was assembled before 3.0 Ga and collided with the Zimbabwe craton to the north at 2.0–2.8 Ga, forming the Limpopo orogenic belt (Figure 1). An intracratonic intrusion, the Bushveld event at 2.05 Ga [*de Wit et al.*, 1992] disrupted the stable Kaapvaal craton and formed the Bushveld Complex in the northern Kaapvaal craton. The Kaapvaal craton is bounded by Proterozoic mobile belts (the Kheiss thrust belt, the Namaqua-Natal belt, and the Limpopo belt) to the west, south, and north, respectively, and by the Lebombo monocline of Jurassic volcanic rocks to the east [*de Wit et al.*, 1992]. The Phanerozoic Cape Fold belt (0.3 Ga) in the southern end of Africa is the youngest part of the southern Africa continent. Although southern Africa is an old continent, it has experienced frequent kimberlite eruptions mostly since the breakup of the Pangean supercontinent began at ~180 Ma. It has been suggested that the kimberlites are associated with major hot spot events, such as the Karoo, Tristan, Kerguelen, and Reunion events [*Crough et al.*, 1980; *Jelsma et al.*, 2004].

[3] Like other continental shield regions, the Kaapvaal craton is characterized by a fast and thick lithosphere as imaged in both global and regional seismic models with a range of lateral and vertical resolutions [*Grand et al.*, 1997; *Ekstrom et al.*, 1997; *Ritsema and van Heijst*, 2000; *James et al.*, 2001; *Fouch et al.*, 2004]. The thickness of the Kaapvaal lithosphere was determined at ~250 km in a regional surface wave model [*Ritsema and van Heijst*, 2000] and in body wave tomography models [*James et al.*, 2001; *Fouch et al.*, 2004] on the basis of the shape and depth extent of high-velocity anomalies. *Rudnick and Nyblade* [1999] constrained the thickness of the Kaapvaal lithosphere at 200–250 km from cratonic xenoliths but the keel thickness could be significantly shallower (150–200 km) if the deformed, high-temperature peridotites were not included. These peridotites have low seismic velocities and are not consistent with the high-velocity root in the tomographic images [*James et al.*, 2004]. *Artemieva and Mooney* [2001] modeled global heat flow data and found that the thermal thickness of the Kaapvaal lithosphere was 175–220 km.

[4] Although southern Africa has frequently experienced hot spot events since 180 Ma, earlier *P* wave velocity models in southern Africa do not show lithosphere thinning or a low-velocity zone in the upper mantle [*Nyblade et al.*, 1996; *Zhao et al.*, 1999; *Simon et al.*, 2002]. Recently, *Wang et al.* [2005] found that a low-velocity zone is required below 150 km in the upper mantle of southern

[1]Department of Geosciences, University of Houston, Houston, Texas, USA.

0148-0227/06/2006JB004321$09.00

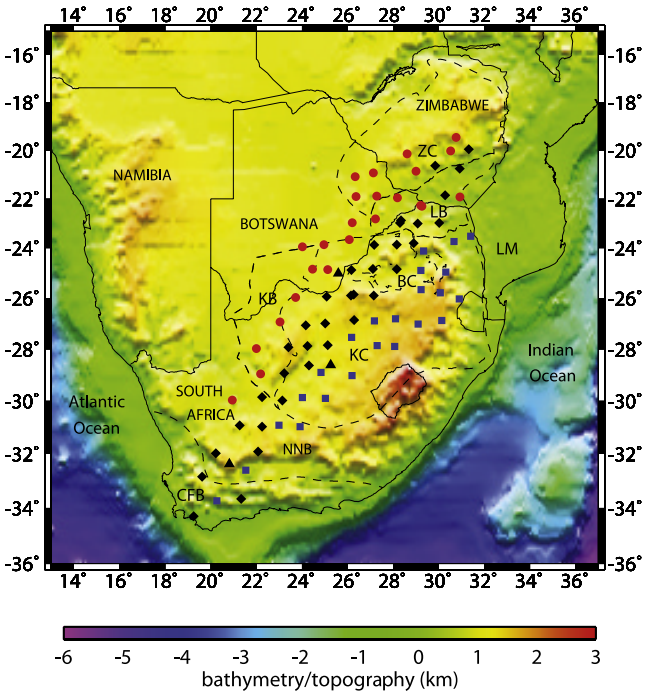

Figure 1. Map of topography and seismic stations in southern Africa. Diamonds are stations that operated for 2 years. Stations at the circles were moved to the sites marked by squares after 1 year of operation. Triangles are long-term stations. Tectonic provinces are outlined by dashed lines. KC, Kaapvaal craton; BC, Bushveld Complex; ZC, Zimbabwe craton; LB, Limpopo Belt, KB, Kheiss Belt; NNB, Namaqua-Natal Belt; CFB, Cape-Fold Belt; LM, Lebombo Monocline.

Africa by modeling *P* and *SH* arrivals from regional earthquakes. Shear wave models constrained from waveform modeling and surface waves have revealed a low-velocity layer under the lithosphere of South Africa [*Qiu et al.*, 1996; *Priestley*, 1999]. On the other hand, *Freybourger et al.* [2001] and *Saltzer* [2002] modeled both Rayleigh and Love waves in southern Africa and constrained a much smoother shear wave model, in which neither a fast lithosphere nor a low-velocity layer was observed. Studies using *P* to *S* converted phases imaged a discontinuity of negative velocity gradient at 300 km depth [*Vinnik et al.*, 1996; *Stankiewicz et al.*, 2002], ~100 km deeper than the low-velocity zone in the shear wave models [*Qiu et al.*, 1996; *Priestley*, 1999]. This discontinuity is not observed in other receiver function studies in southern Africa [*Gao et al.*, 2002; *Niu et al.*, 2004].

[5] A characteristic feature of southern Africa is an anomalously high surface topography of 1 to 2 km (Figure 1). How the high elevation is compensated remains debatable. *Webb et al.* [2004] have shown that surface loads at many stations in southern Africa are undercompensated by crustal variations. The low seismic velocities imaged in the lower mantle (the Africa superplume) [*Ritsema et al.*, 1998; *Ni et al.*, 2002] have been considered to generate dynamic topography, but the predicted amplitude is much lower than the observed elevations [*Lithgow-Bertelloni and Silver*, 1998]. The contribution of the lower mantle to surface topography in southern Africa is probably even less if the very low velocity anomaly in the lower mantle is attributed to variation in composition [*Ni et al.*, 2002]. *Simon et al.* [2002] observed relatively high wave speeds in the transition zone under the southern part of southern Africa and suggested that they may be due to iron depletion and contribute to the surface elevation. This observation contradicts a receiver function study that imaged a flat low-velocity layer in the transition zone of southern Africa [*Shen and Blum*, 2003]. Heating and buoyancy in the upper mantle of southern Africa has been proposed to support the high surface relief [*Nyblade and Robinson*, 1994; *Burke*, 1996; *Burke et al.*, 2003]. The absence of convincing seismic evidence in the southern Africa upper mantle has been a problem for these models.

[6] In this study, we developed a high-resolution, 3-D, shear wave model for southern Africa using fundamental mode Rayleigh waves recorded at the stations of the southern Africa Seismic Experiment (SASE) [*Carlson et al.*, 1996]. Our model imaged a high-velocity keel of the Kaapvaal craton to the depths of 180 ± 20 km. A weak low-velocity zone (LVZ) is observed for the first time at 160 to 260 km depths across nearly all of southern Africa. The velocity in this layer varies from 4.45 km/s under the Namaqua belt to ~4.6 km/s under the central Kaapvaal craton. The image of this LVZ is important in determining the keel depth and has significant implications for dynamic processes in southern Africa.

2. Data Selection and Analysis

[7] We utilized Rayleigh waves recorded at the SASE stations, which operated from April 1997 to July 1999. The SASE array consisted of 82 broadband seismic stations and was deployed across southern Africa from the Cape Fold belt in southwest to the Zimbabwe craton in northeast (Figure 1). Thirty-two stations continuously recorded data during the 2-year experiment, and 23 stations were moved to different locations after the first year. Three long-term stations in southern Africa from the Global Seismic Network are also used in our analyses.

[8] Teleseismic events were selected with magnitudes $\geq$ 5.8 and epicentral distances between 20° and 120° from the center of the array. Over 200 events are available for surface wave analyses. After carefully examining waveforms, 80 events that produced high-quality Rayleigh wave data were used in the final data set. These events showed a good azimuthal coverage in general with a slightly poor coverage to the south (Figure 2). Raypaths are dense within the array and in the surrounding regions except to the southeast of the array (Figure 3).

[9] We corrected instrument responses by converting them to the same type. Vertical component seismograms were filtered at 18 frequencies ranging from 6 to 50 mHz with a Butterworth filter of a 10 mHz bandwidth. We checked data quality by comparing waveforms at nearby stations. Data with bad timing and clipped amplitude can be identified by this process and only waveforms that showed good correlations among nearby stations were kept in the data set. In general, short-period Rayleigh waves from earthquakes at very long distances are complicated and not consistent from station to station, and long-period

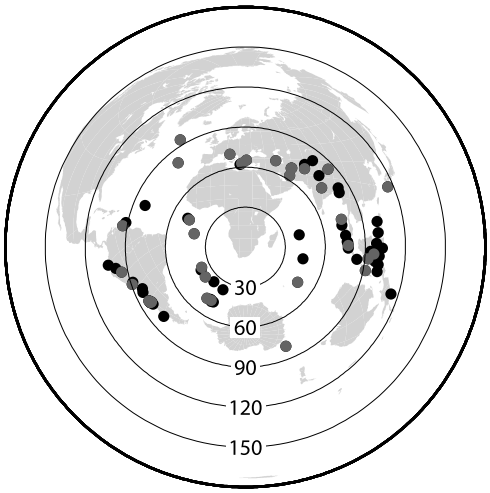

Figure 2. Distribution of teleseismic events (solid circles) used in this study. Gray circles represent the events that are used to generate raypaths shown in Figure 3. Epicentral distance from the center of the seismic array is marked by large circles with numbers.

Rayleigh waves from relatively small earthquakes are noisy on seismograms. Our final data set consists of ~36,000 Rayleigh wave trains. The phases and amplitudes of Rayleigh waves are calculated using a Fourier transform approach and are normalized relative to a reference station for each event.

3. Methodology

[10] We adopted a two-step inversion procedure in this Rayleigh wave tomography study. At the first step, a two-plane wave inversion technique [*Li et al.*, 2003; *Forsyth and Li*, 2005] is used to obtain phase velocities in southern Africa. The two-plane wave method can account for the effects of structure outside the study area by representing an incoming wavefield as the interference of two plane waves with different amplitudes, phases, and propagation directions. The parameters of the two plane waves are first estimated in the inversion using a simulated annealing approach and then solved simultaneously with phase velocities in a generalized linear inversion. For events whose incoming wavefields are too complex to be fully represented by two plane waves, we assigned them large errors and small weighting factors to reduce their influence in the final model. The study area was parameterized with 783 nodes (Figure 4). Phase velocities are allowed to vary at each node in 2-D inversions and a characteristic length of 80 km is used to smooth phase velocity models. We assigned an a priori error of 0.25 km/s to model parameters (phase velocity) at the inner nodes and 2.5 km/s at the edge nodes (the most outside two rows and columns) so that any wavefield caused by the heterogeneity along a raypath that cannot be represented by the two plane waves is largely "absorbed" at the edges. Corrections for site effect and attenuation at each station are solved in the first round phase velocity inversions and then applied to the Rayleigh wave data. Rayleigh waves with these corrections are inverted again for phase velocities.

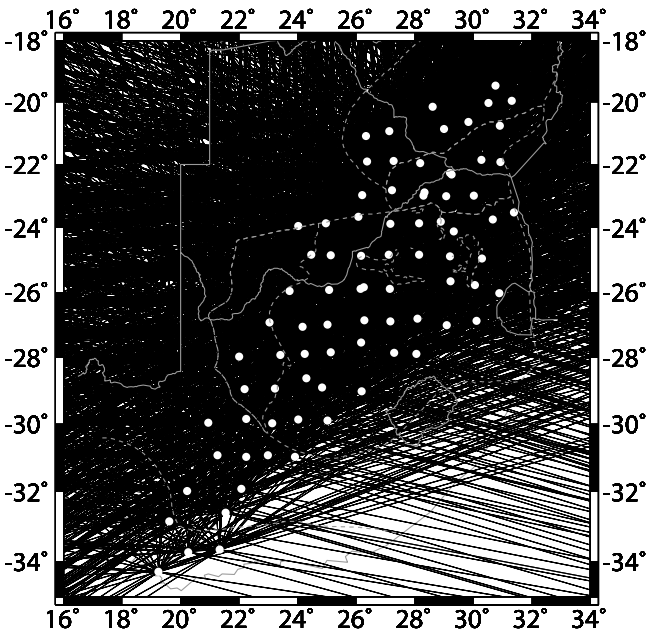

Figure 3. Great circle raypaths from 32 events (gray circles in Figure 2), less than half of the total available events. Raypath coverage within the station array is excellent. The coverage is relatively poor to the southeast of the array.

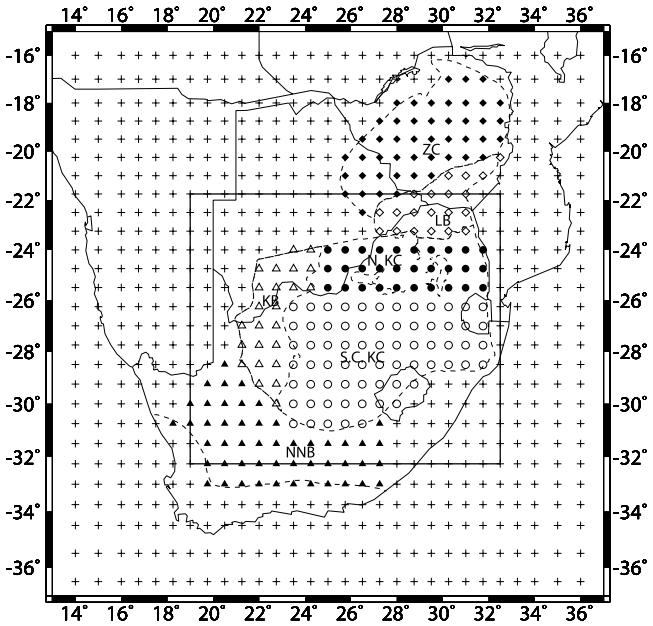

Figure 4. Grid nodes in the study area. Different symbols are used for six different tectonic provinces (solid triangles for the Namaqua-Natal Belt, open triangles for the Kheiss Belt, open circles for the southern and central Kaapvaal craton, solid circles for the northern Kaapvaal craton, open diamonds for the Limpopo Belt, and solid diamonds for the Zimbabwe craton). Crosses are the locations of nodes outside the station array. The inside rectangle outlines the area in which a test inversion was performed to investigate how Rayleigh wave solutions are affected by the dimensions of the array.

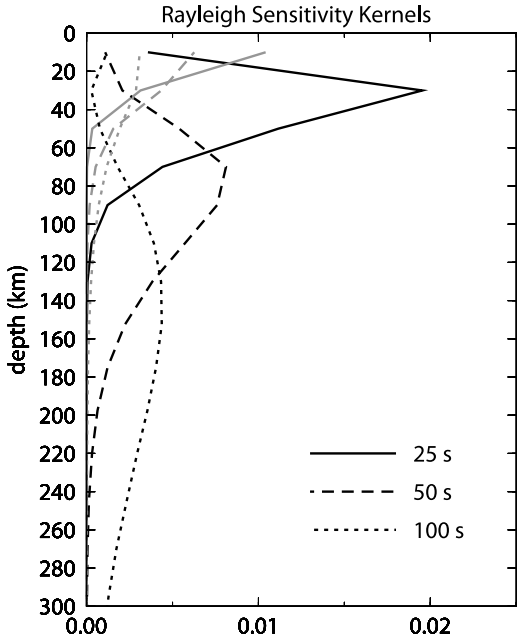

Figure 5. Rayleigh wave sensitivity kernels at periods of 25 s (solid lines), 50 s (long-dashed lines), and 100 s (short-dashed lines). Black lines represent partial derivatives of $\partial c/\partial v_s$, and gray lines represent $\partial c/\partial v_p$.

[11] We performed a second step inversion to solve for shear wave structure from the determined phase velocities. Model parameters in this inversion are shear wave velocities in 16 layers from the Earth's surface to 410 km depth. Velocities below 410 km are fixed values from the model AK135 [*Kennett et al.*, 1995]. We adopted the method of *Saito* [1988] to calculate the derivatives of phase velocities with respect to model parameters, which can be written as $dc/d\beta = \partial c/\partial\beta + (\partial c/\partial\alpha)(\partial\alpha/\partial\beta) = \partial c/\partial\beta + \sqrt{3}(\partial c/\partial\alpha)$, where α, β, and c are P wave, S wave, and Rayleigh wave velocity, respectively. Rayleigh waves are primarily sensitive to shear wave structure with the maximum sensitivity depth at ~1/3 of a given wavelength. Their sensitivity to P wave structure is confined at very shallow depths (<50 km) even at longer periods (Figure 5). We therefore only constrained shear wave structure in southern Africa. A Vp/Vs ratio of $\sqrt{3}$ is applied in the inversions for calculating the total derivatives and the P wave models. Although such a Vp/Vs ratio may not be appropriate for the mantle structure, it should not affect the obtained shear wave velocities because of the insensitivity of Rayleigh waves to P wave structure at greater depths.

[12] Because correlation exists between phase velocities at nearby periods, the inversion for shear wave structure is an underdetermined inverse problem although the total number of data (phase velocities at 18 periods) is greater than the total number of model parameters (shear wave velocities in 16 layers). We used the approach of generalized inversion in solving for shear wave structure from Rayleigh wave dispersions. The AK135 model [*Kennett et al.*, 1995] is used as the initial model. A correlation coefficient of 0.3 was assigned between adjacent layers to smooth the model. We placed an a priori standard error of 0.1 km/s in each model parameter. This value was determined after several experiments with different values from 0.05 to 0.25 km/s. We have found that strong oscillations between adjacent layers can occur if using a large standard error, say 0.25 km/s. Our criterion is to have a model that is smooth and also varies as much as possible from the starting model.

4. Phase Velocities

[13] We first calculated average phase velocities in the whole study area and in six tectonic provinces including the Namaqua-Natal Belt, the Kheiss Belt, the southern and central Kaapvaal craton, the northern Kaapvaal craton, the Limpopo belt, and the Zimbabwe craton. These provinces are indicated in Figure 4 by different symbols. Average phase velocities in southern Africa range from 3.654 ± 0.001 km/s at 20 s to 4.454 ± 0.008 km/s at 167 s (Figure 6), which are similar to but slightly higher than Rayleigh phase velocities of the Kaapvaal craton in the global model [*Ekstrom et al.*, 1997]. The average dispersion curve in southern Africa well represents the dispersions in the provinces of the Kaapvaal and Zimbabwe cratons and the Limpopo mobile belt. Phase velocities in the Namaqua-Natal belt are ~2% lower than the averages in southern Africa. The highest Rayleigh wave phase velocities at periods less than 100s are observed in the southern and central Kaapvaal craton and the Zimbabwe craton, while at longer periods, the northern Kaapvaal craton and the Limpopo belt are characterized by higher phase velocities.

[14] Lateral variations of phase velocities in southern Africa were solved at each grid node. The average phase velocities were used as starting values in 2-D inversions. We generated fine-grid ($0.1^\circ \times 0.1^\circ$) maps of phase velocity by applying a Gaussian smoothing with a characteristic length of 80 km to the solutions in the original grid. Phase velocity perturbations computed relative to the average phase velocities in the study area are shown in Figure 7 at periods of 25, 40, 50, 67, 100, and 125 s. Rayleigh wave phase velocities correlate well with the tectonic provinces in southern Africa. Fast anomalies appear in the Kaapvaal and Zimbabwe cratons and slow anomalies are imaged in the Bushveld Complex area and in the surrounding mobile belts. Phase velocities at 40 s reflect more on crustal thickness variation, indicating that crust is thin in the cratons and thicker in the mobile belts, consistent with Moho depths constrained from receiver functions [*Nguuri et al.*, 2001; *James et al.*, 2003]. Fast anomalies at the intermediate to long periods manifest as disconnected patches, indicating that lateral variations exist in the Kaapvaal cratonic lithosphere.

5. Uncertainties and Resolution of Phase Velocities

[15] Several factors contribute to uncertainties in the resolved phase velocities. Like all inverse problems, uncertainties in Rayleigh wave data are the most direct cause of errors in phase velocity solutions. Because the same error in phase corresponds to a larger error in time at a longer period, errors in absolute phase velocity generally increase with period. The standard errors of phase velocity are calculated in the inversions. Because both phase velocity

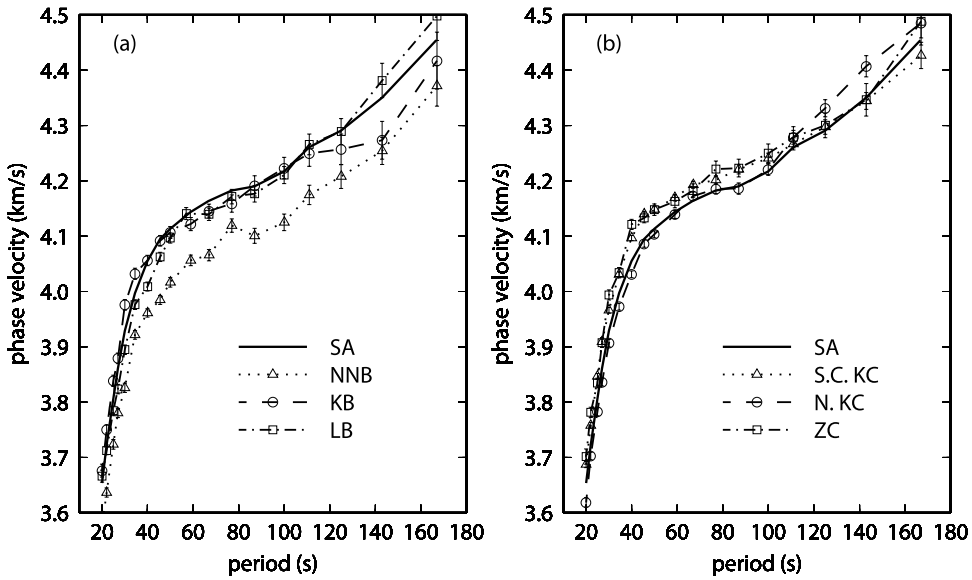

Figure 6. Average Rayleigh wave dispersions in southern Africa (solid lines) and in six subregions (dashed lines and symbols) of the study area. (a) Phase velocities for the regions of mobile belts (the Namaqua-Natal, the Kheiss, and the Limpopo belts). (b) Phase velocities for the cratons (the Kaapvaal and Zimbabwe cratons). KB, LB, NNB, and ZC have the same meaning as defined in Figure 1. S.C. KC, southern and central Kaapvaal craton; N. KC, northern Kaapvaal craton; SA, southern Africa.

and its standard error increase with period, their ratio, the error of phase velocity perturbation, is less dependent on period. The error contours in phase velocity perturbation tend to elongate along the long axis of the SASE array in NNE and SSW direction (Figure 7c), and the errors are small near the center of the array and become large with distance away from the array.

[16] It has been known that there is tradeoff between azimuthal anisotropy and lateral heterogeneity. Since our inversions are isotropic, the question is how the solutions of isotropic phase velocity are affected by ignoring anisotropy. We believe that such an effect is small and does not affect the observed pattern of isotropic phase velocities. One reason is that azimuthal anisotropy is largely averaged out in the inversions because of the dense crossing raypaths. Another reason is that the magnitude of anisotropy is small in the upper mantle of southern Africa according to shear wave splitting results [*Silver et al.*, 2001]. We have solved for phase velocities and azimuthal anisotropy simultaneously in southern Africa and found that anisotropy is weak in the Kaapvaal craton, consistent with shear wave splitting observations. Results about anisotropy from Rayleigh waves will be discussed in a different paper.

[17] Another contributor to the errors in phase velocity solutions could be the validation of the two-plane wave method. One assumption in the approach is that the initial phases at all stations from one event are the same, which is valid when the aperture of the array corresponds to a small azimuthal angle at the source. Since the SASE array is large, it seems more accurate to apply the method by dividing the array to two subareas. We are not convinced for the necessity of doing so by the following reasons. First, the seismic array is only long in the NE-SW direction and only the events from the northwest or southeast could have this potential problem. This problem is even trivial considering that the majority of events have distances beyond 70°. Second, the parameters for the two plane waves are solved in the inversions, which can partially account for the inaccuracy in this assumption on the same initial phase. Furthermore, we have performed a test on this issue by using the stations only in the Kaapvaal craton and running the inversion in a much smaller region as indicated by the rectangle in Figure 4. Our experiment shows that the difference of phase velocity in the Kaapvaal craton between this inversion and the inversion applied in the whole array is negligible except at the edges. We therefore conclude that the same-initial-phase assumption in the two-plane wave method is largely valid and does not pose notable bias to the phase velocity solutions in southern Africa.

[18] To investigate how well phase velocities in southern Africa are resolved, we have conducted resolution tests for checkerboard models at periods of 50 s, 100 s, and 125 s (Figure 8). Synthetic phase and amplitude data of Rayleigh waves were generated for a checkerboard model with fast and slow anomalies of 2.5% on a length scale of ~250 km. The events and stations used in producing the synthetic data are same as in the real data. The checkerboard pattern and the amplitude of the anomalies can be well recovered at 50 s and 100 s. Although lateral bleeding is more developed at 125 s, the anomalies are still resolvable in the area where more stations are located. The reduction of lateral resolution at longer periods is partially due to the finite-frequency effect. This effect can be reduced in future studies by applying an improved two-plane wave method with finite frequency kernels [*Yang and Forsyth*, 2006].

6. Shear Wave Structure of Southern Africa

6.1. One-Dimensional Shear Wave Structure

[19] One-dimensional shear wave structure beneath southern Africa is constrained by inverting average Rayleigh wave phase velocities. In this inversion, we assumed a

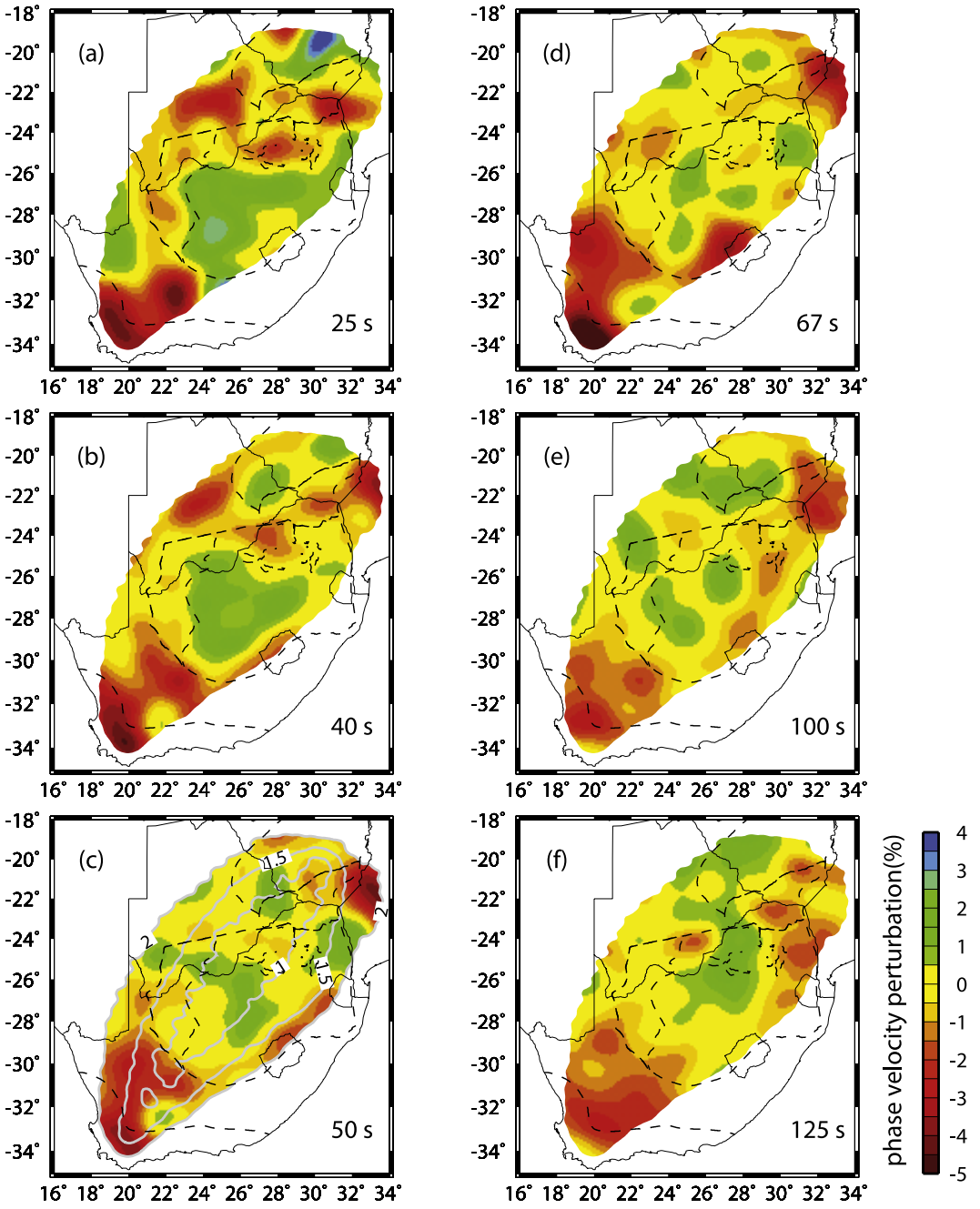

Figure 7. Maps of Rayleigh wave phase velocity perturbations in southern Africa at the periods of (a) 25 s, (b) 40 s, (c) 50 s, (d) 67 s, (e) 100 s, and (f) 125 s. The perturbations are relative to the average phase velocities in southern Africa. The maps are clipped using the contour of 2% standard deviations for phase velocity perturbations at a period of 50 s (gray lines in Figure 7c).

40 km thick crust on the basis of the Moho depths at the SASE stations determined from receiver functions [*Nguuri et al.*, 2001]. Crustal thickness can trade off with velocity near the Moho (20–60 km) while the trade-off is negligible at other depths. The model AK135 is used as a starting model in the inversion. We also performed the inversion with different initial models and found that their effect on the optimum model solution is trivial.

[20] The resolution to shear wave velocity decreases with depth in general. As shown in Figure 9, peak values in the model resolution matrix become smaller at greater depths. There are total six pieces of independent information in this inversion, about 2.5 for velocity at the depths of 40 to 165 km, and ~1 at the depths of 165–260 km and 260–410 km, respectively. Although velocities in each layer cannot be perfectly resolved, the average velocity can be well determined at the depth ranges of 50 km, 100 km, and 150 km from the shallow to the lower upper mantle.

[21] A fast mantle lid is imaged to the depth of ~180 km with a shear wave velocity of ~4.67 km/s (Figure 10). A weak low-velocity zone exists beneath the mantle lid to the depth of 260 km, and the average velocity in the LVZ is

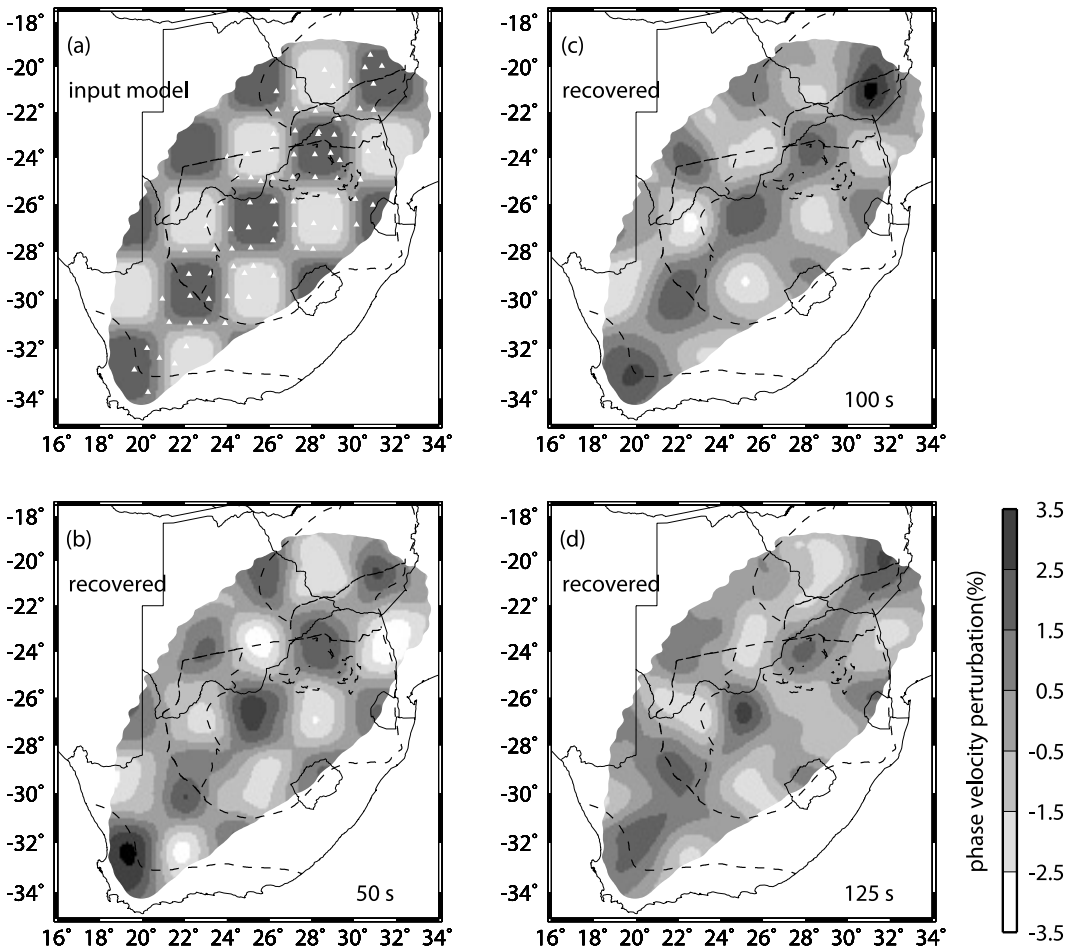

Figure 8. Resolution test for Rayleigh wave phase velocities in southern Africa. (a) Input model with 2.5% anomalies in a checkerboard pattern. (b–d) Recovered models at periods of 50 s, 100s, and 125 s.

4.48 km/s. This velocity is not absolutely low compared to the global model of AK135, but it is over ~4% lower than the fast mantle lid above. The fast lid is not only imaged in our and other shear wave models [*Qiu et al.*, 1996; *Priestley*, 1999] but also evidenced by xenolith studies in southern Africa [*James et al.*, 2004]. For example, shear wave velocities from cratonic mantle xenoliths in southern Africa vary from 4.71 km/s at 50 km depth to 4.65 km/s at 170 km [*James et al.*, 2004], which almost perfectly agree with our velocity profile in Figure 10.

[22] The fast lid and the weak LVZ imaged in our model are compatible with the model of *Priestley* [1999]. Our 1-D model is significantly different from the model of *Qiu et al.* [1996] in which an LVZ is much stronger and shallower. Our model is not consistent with the 1-D transverse isotropic models given by *Freybourger et al.* [2001] and *Saltzer* [2002]. Their models are much smoother with depth and do not reveal a fast lid at all. Although *Saltzer* [2002] found that an artificial low-velocity layer could arise from inverting anisotropic data of Rayleigh and Love waves for an isotropic model. This argument is not applicable if only Rayleigh wave data are used. The discrepancy between the isotropic and anisotropic models is still not well understood.

[23] One-dimensional shear wave velocity models for six subregions in southern Africa (Figure 11) are obtained from

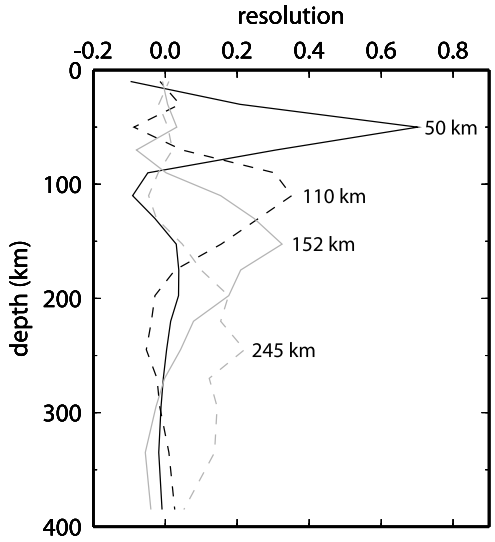

Figure 9. Rows of the resolution matrix corresponding to four layers with median depths at 50, 110, 152, and 245 km. A peak value at the corresponding depth indicates good resolution. The sharper the peak is, the higher the resolution for that layer.

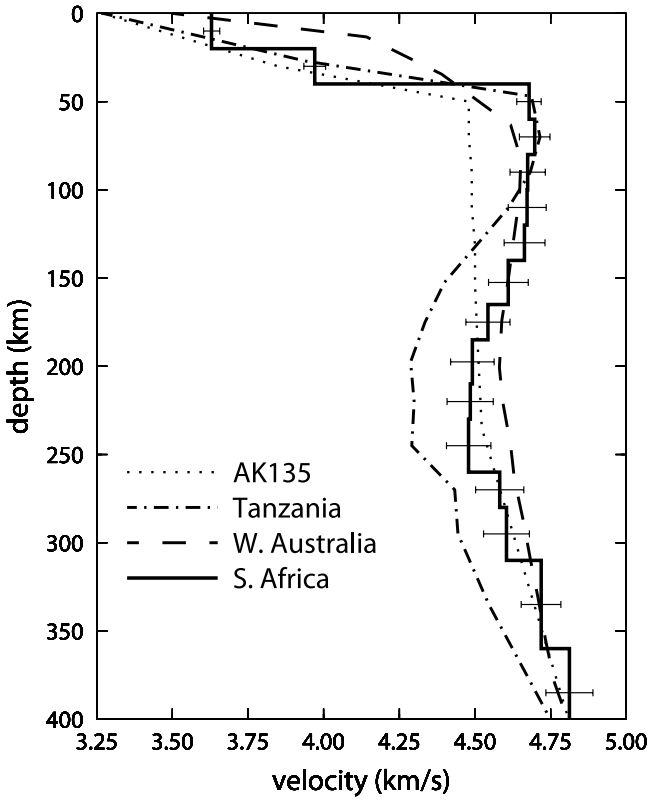

Figure 10. (a) One-dimensional shear wave velocity in southern Africa (solid line) with standard errors. Shear wave profiles in the Tanzanian craton (dash-dotted line) [*Weeraratne et al.*, 2003], the western Australian craton (dashed line) [*Simons et al.*, 1999], and the AK135 model (dotted line) [*Kennett et al.*, 1995] are plotted for comparison.

their corresponding average Rayleigh wave dispersions (Table 1). According to the receiver function results [*Nguuri et al.*, 2001], we fixed the crustal thickness in the inversions at 46 km for the Namaqua-Natal belt, 36 km for the Kheiss belt, 40 km for the southern and central Kaapvaal, 43 km for the northern Kaapvaal, 45 km for the Limpopo belt, and 38 km for the Zimbabwe craton. We observed a fast mantle lithosphere and significant velocity reductions beneath it in all the tectonic provinces of southern Africa. The lithosphere lid thins from ~180 km in the Kaapvaal craton to ~80 km in the Namaqua-Natal belt toward south and to ~120 km in the Zimbabwe craton toward north. Another difference among these models is the velocity in the deep upper mantle below 260 km. Shear wave velocity at the depths of 260 to 400 km is much lower in the south including the Namaqua-Natal belt, the Kheiss belt, and the southern and central Kaapvaal craton than in the northern part of southern Africa. On the other hand, the upper mantle below 260 km is remarkably fast beneath the northern Kaapvaal craton (Figure 11e). Such large regional variations in shear wave structure in southern Africa might help to explain the differences in previous models [*Qiu et al.*, 1996; *Priestley*, 1999; *Freybourger et al.*, 2001; *Saltzer*, 2002] if they are associated with different parts of southern Africa.

[24] To examine the robustness of the fast lid and the LVZ in the shear wave model of southern Africa, we conducted a series of experiments of forward modeling through models that have variable velocities and thicknesses for the lid and the LVZ (Figure 12). Models without an LVZ cannot fit the dispersion curve regardless of the velocity in the shallow upper mantle. Simply removing the LVZ from the average southern Africa model makes predicted phase velocities beyond the period of 70 s much faster than those observed (Figures 12a and 12b). If the lid and the LVZ are replaced with an average velocity at the depths of 40 to 260 km, the model predicts much lower phase velocities at periods <80 s (Figures 12a and 12b). These tests demonstrate that a fast lid and an LVZ are required by the data.

[25] Because of nonuniqueness in model solutions and because of errors in phase velocity measurements, there are still infinite numbers of models that can fit the data at some degrees. For example, a model with a thicker and weaker LVZ and a model with an LVZ about 40 km deeper also fit the dispersion curve reasonably well (Figures 12c–12f). However, the curvature of phase velocity around the periods of 80–100 s is not well predicted from both models. Models with a strong LVZ or a shallow LVZ tend to predict phase velocities lower than the observations. Our experiments show that it is difficult to distinguish models with ±20 km changes in the lid thickness or with ±0.05 km/s changes in the average velocity of the LVZ relative to the most favorable model in Figure 10.

6.2. Three-Dimensional Shear Wave Structure

[26] We have applied the same inversion technique used in the 1-D inversion to each map point to obtain 3-D shear wave structure in southern Africa. The crustal thickness was fixed in the inversions at each map point and its value was estimated by interpolating the crustal thickness at the SASE stations constrained from receiver functions [*Nguuri et al.*, 2001]. As discussed above, uncertainties of crustal thickness can affect velocity in the lower crust and uppermost mantle but their influence on mantle structure below 80 km is negligible.

[27] Three-dimensional variations of shear wave structure in the southern Africa upper mantle are presented on maps and vertical profiles in Figures 13, 14, and 15. The southern boundary of the Kaapvaal craton is marked by a sharp velocity drop of 0.2 km/s from the Kaapvaal craton to the Namaqua belt (Figure 13). Within the Kaapvaal lithosphere, the Bushveld Complex area is relatively slower than the rest of the craton (Figures 14a–14c), probably associated with high iron content from the Bushveld intrusion at 2.05 Ga. A fast mantle lid is present beneath most of the cratons and mobile belts except the western Namaqua mobile belt and the Cape Fold belt. The fast mantle lithosphere varies from 140 ± 20 km at the edges of the Kaapvaal craton to 180 ± 20 km near its center (Figures 14a, 15c, and 15d) on the basis of velocity contours of 4.55 km/s and 4.6 km/s. The maximum keel depth in our model is ~210 km, corresponding roughly to the average depth to the middle of the LVZ, which is slightly shallower than in previous tomography models [*Ritsema and van Heijst*, 2000; *James et al.*, 2001; *Fouch et al.*, 2004]. Such a difference comes from different criteria that are used to determine the keel depth rather than from real differences among the models. More discussions on this problem are given in section 7.

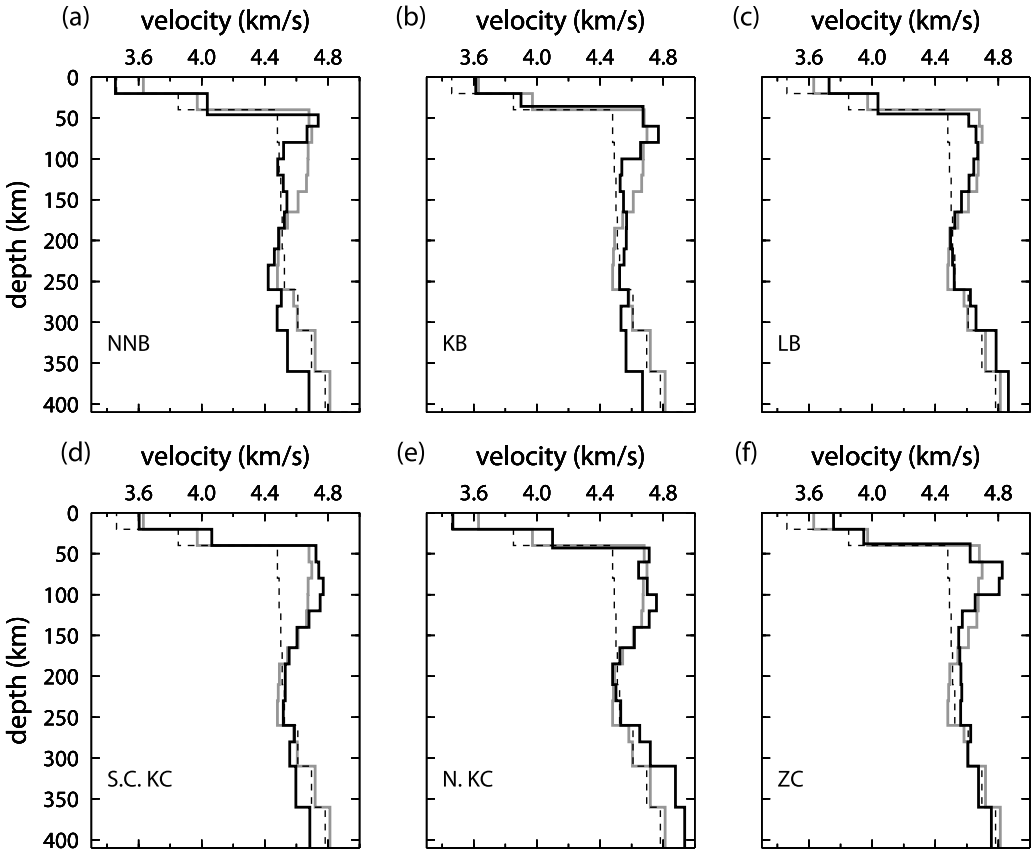

Figure 11. One-dimensional shear wave velocity profiles in six subregions (black solid lines) in southern Africa including (a) the Namaqua-Natal belt, (b) the Kheiss belt, (c) the Limpopo belt, (d) the southern and central Kaapvaal craton, (e) the northern Kaapvaal craton, and (f) the Zimbabwe craton. The AK135 model (dashed line) [*Kennett et al.*, 1995] and the average southern Africa model (gray line) are plotted for reference.

[28] Figures 14b and 14c are velocity perturbation profiles relative to the average southern Africa model and the AK135 model [*Kennett et al.*, 1995], respectively. Since the reference model of southern Africa contains a fast lid, more negative anomalies appear in Figure 14b above 200 km. The slow anomalies concentrate in regions under the border areas between tectonic provinces. Relatively slow anomalies are also imaged under the Bushveld Complex to the depth of 150 km, which seems connected to stronger negative anomalies under the Limpopo belt and the Zim-

Table 1. Rayleigh Wave Phase Velocities in Southern Africa and Six Subregions[a]

Period, s	Average SA, km/s	NNB, km/s	KB, km/s	LB, km/s	S.C. KC, km/s	N. KC, km/s	ZC, km/s
20.0	3.654 ± 0.001	3.575 ± 0.005	3.676 ± 0.006	3.666 ± 0.005	3.687 ± 0.003	3.619 ± 0.004	3.702 ± 0.007
22.2	3.723 ± 0.001	3.637 ± 0.004	3.750 ± 0.005	3.713 ± 0.004	3.758 ± 0.003	3.703 ± 0.003	3.782 ± 0.004
25.0	3.806 ± 0.001	3.724 ± 0.004	3.838 ± 0.005	3.785 ± 0.004	3.847 ± 0.003	3.783 ± 0.004	3.834 ± 0.004
27.0	3.861 ± 0.001	3.780 ± 0.004	3.879 ± 0.005	3.824 ± 0.004	3.909 ± 0.002	3.836 ± 0.003	3.908 ± 0.004
30.3	3.929 ± 0.001	3.826 ± 0.004	3.976 ± 0.005	3.895 ± 0.004	3.966 ± 0.003	3.907 ± 0.003	3.994 ± 0.005
34.5	3.997 ± 0.001	3.922 ± 0.004	4.032 ± 0.005	3.976 ± 0.004	4.031 ± 0.002	3.972 ± 0.003	4.034 ± 0.005
40.0	4.055 ± 0.001	3.961 ± 0.004	4.056 ± 0.005	4.009 ± 0.004	4.097 ± 0.002	4.031 ± 0.003	4.121 ± 0.005
45.5	4.095 ± 0.001	3.985 ± 0.004	4.092 ± 0.005	4.063 ± 0.004	4.140 ± 0.002	4.086 ± 0.003	4.133 ± 0.005
50.0	4.113 ± 0.001	4.017 ± 0.004	4.107 ± 0.005	4.097 ± 0.005	4.148 ± 0.003	4.103 ± 0.003	4.148 ± 0.005
58.8	4.143 ± 0.001	4.056 ± 0.005	4.122 ± 0.006	4.141 ± 0.005	4.170 ± 0.003	4.139 ± 0.004	4.163 ± 0.006
66.7	4.163 ± 0.002	4.066 ± 0.005	4.146 ± 0.006	4.140 ± 0.006	4.193 ± 0.003	4.172 ± 0.004	4.182 ± 0.006
76.9	4.183 ± 0.002	4.119 ± 0.006	4.159 ± 0.008	4.171 ± 0.007	4.202 ± 0.004	4.185 ± 0.004	4.221 ± 0.007
86.9	4.190 ± 0.002	4.101 ± 0.007	4.191 ± 0.009	4.177 ± 0.007	4.221 ± 0.004	4.186 ± 0.005	4.223 ± 0.008
100.0	4.217 ± 0.003	4.125 ± 0.007	4.223 ± 0.010	4.210 ± 0.008	4.241 ± 0.005	4.220 ± 0.005	4.250 ± 0.008
111.1	4.261 ± 0.003	4.175 ± 0.009	4.250 ± 0.012	4.266 ± 0.009	4.267 ± 0.005	4.279 ± 0.006	4.279 ± 0.010
125.0	4.291 ± 0.004	4.208 ± 0.011	4.257 ± 0.014	4.289 ± 0.012	4.297 ± 0.007	4.331 ± 0.008	4.300 ± 0.011
142.9	4.350 ± 0.005	4.254 ± 0.012	4.273 ± 0.017	4.381 ± 0.015	4.344 ± 0.008	4.407 ± 0.010	4.346 ± 0.015
166.7	4.454 ± 0.008	4.372 ± 0.018	4.417 ± 0.026	4.498 ± 0.022	4.427 ± 0.012	4.485 ± 0.013	4.488 ± 0.022

[a]The abbreviations for the tectonic provinces are as follows: SA, southern Africa; NNB, Namaqua-Natal Belt; KB, Kheiss Belt; LB, Limpopo Belt; S.C. KC, southern and central Kaapvaal craton; N. KC, northern Kaapvaal craton; ZC, Zimbabwe craton. Their geographical locations are indicated in Figure 4. Elements in the table are phase velocities with 1 standard deviation.

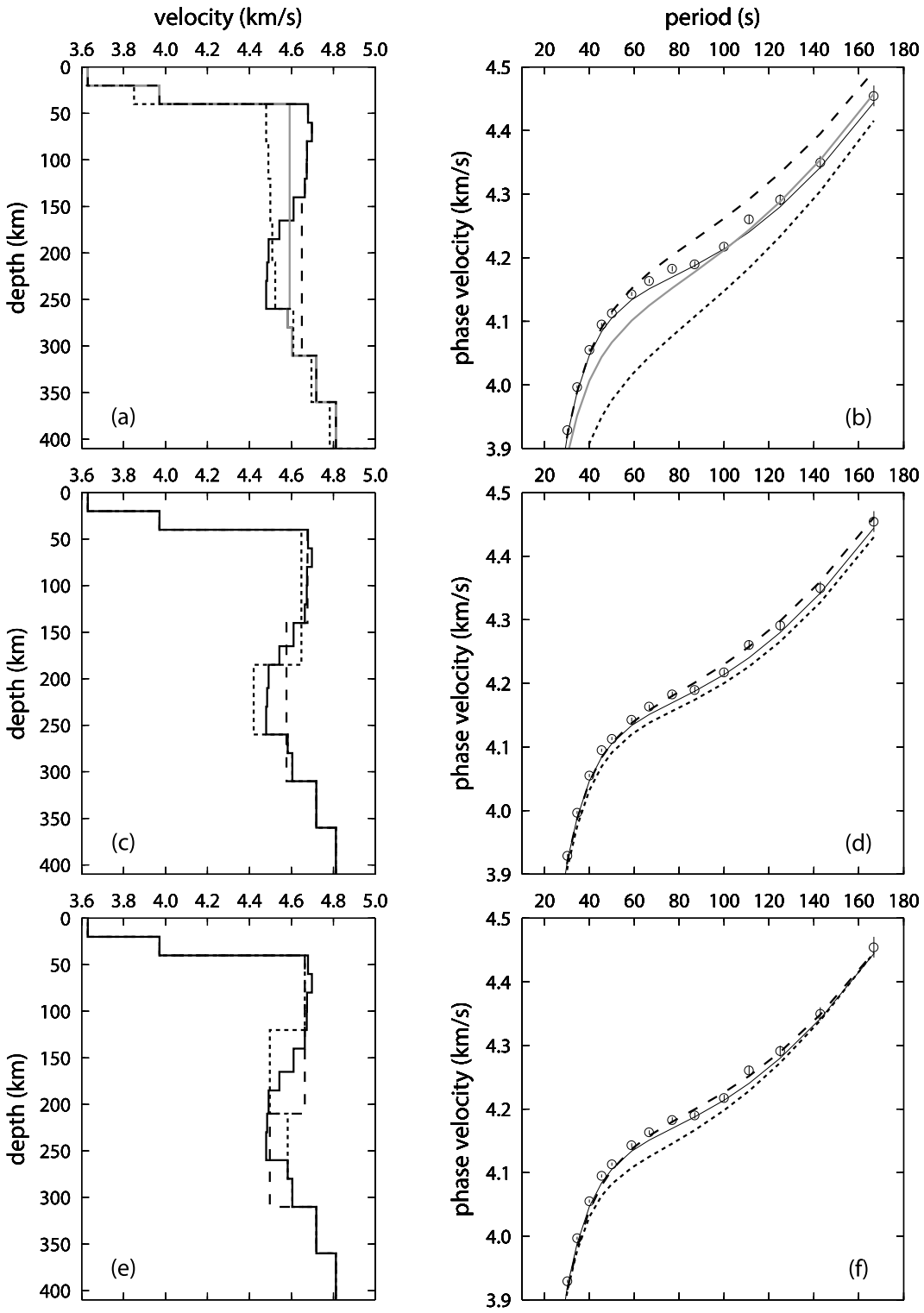

Figure 12. Shear wave models with variable velocity and thickness in the lid and the low-velocity zone (Figures 12a, 12c, and 12e) and their associated Rayleigh wave phase velocities (Figures 12b, 12d, and 12f). Line styles for the velocity models are consistent with those for the phase velocities. The black solid lines in Figures 12a, 12c, and 12e indicate the shear wave model for southern Africa from the inversion of the average phase velocities, which are plotted as circles in Figures 12b, 12d, and 12f with error bars for 1 standard deviation. Short-dashed lines in Figures 12a and 12b are for the model AK135. Gray solid lines and long-dashed lines in Figures 12a and 12b are for two models without an LVZ. Short- and long-dashed lines in Figures 12c and 12d are for models with a strong and thin LVZ and a weak and thick LVZ, respectively. In Figures 12e and 12f, short-dashed lines are for a model with a shallow LVZ and long-dashed lines are for a deep LVZ.

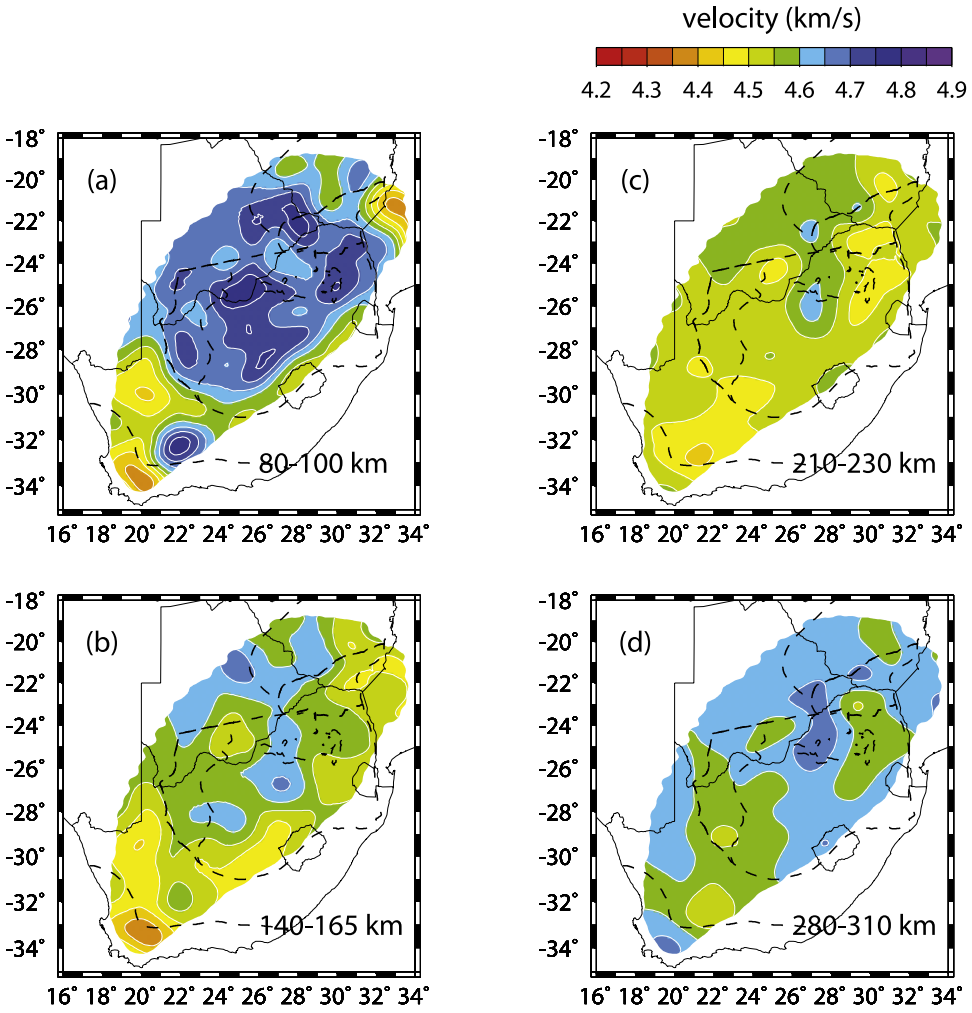

Figure 13. Maps of shear wave velocity in southern Africa in four layers at the depths of (a) 80–100 km, (b) 140–165 km, (c) 210–230 km, and (d) 280–310 km.

babwe craton to the northeast, suggesting that the Bushveld intrusion is probably not from a deep source. Fast anomalies relative to the AK135 model (Figure 14c) reveal a similar pattern to the absolute fast velocities (Figure 14a) above 200 km. A broad negative anomaly below 200 km is imaged beneath the Namaqua mobile belt and the southwestern edge of the Kaapvaal craton. Positive anomalies under the center of the Kaapvaal craton extend all the way to ~400 km depth.

[29] Another interesting feature in our shear wave model is a reduced velocity layer in the upper mantle across southern Africa. This layer can be well perceived in Figure 13, where the layer of 210–230 km is clearly slower than the layer of 80–100 km above and the layer of 280–310 km below. The LVZ is more obvious on the absolute velocity profiles (Figures 14a and 15). It is imaged at the depths of 160 to 260 km with variable strength and thickness. Shear wave velocity in the LVZ varies from 4.45–4.5 km/s under the Namaqua and the Limpopo mobile belts to 4.5–4.6 km/s beneath most of the Kaapvaal craton. A relatively fast block of 4.6–4.65 km/s in the LVZ is imaged in the central and northern Kaapvaal craton near the western Bushveld Complex. Under the Kaapvaal craton, the LVZ is not absolutely low because a shear wave velocity of 4.5–4.6 km/s is compatible with or slightly higher than in a global reference model at the same depths. However, these velocities are ~4% lower compared with the fast keel above the LVZ. It is important to notice that the LVZ does not appear on both velocity perturbation profiles shown in Figure 14 although it is obvious on the absolute velocity profiles. This low-velocity layer and its variable strength across southern Africa are imaged for the first time in a 3-D version. Their importance in understanding the geodynamics of southern Africa is discussed in section 7.2.

7. Discussion

7.1. Kaapvaal Cratonic Lithosphere

[30] The fast cratonic lithosphere is generally attributed to cold temperatures and iron depletion that together make a continental keel mechanically strong and neutrally buoyant [*Jordan*, 1975, 1978, 1979, 1988], which provides a good explanation for the stability of cratons. However, large plume events and tectonic activities can intervene and destroy the strong cratonic lithosphere over time. The most direct evidence is that globally only a small portion of Archaean continent is preserved at the present time. Other

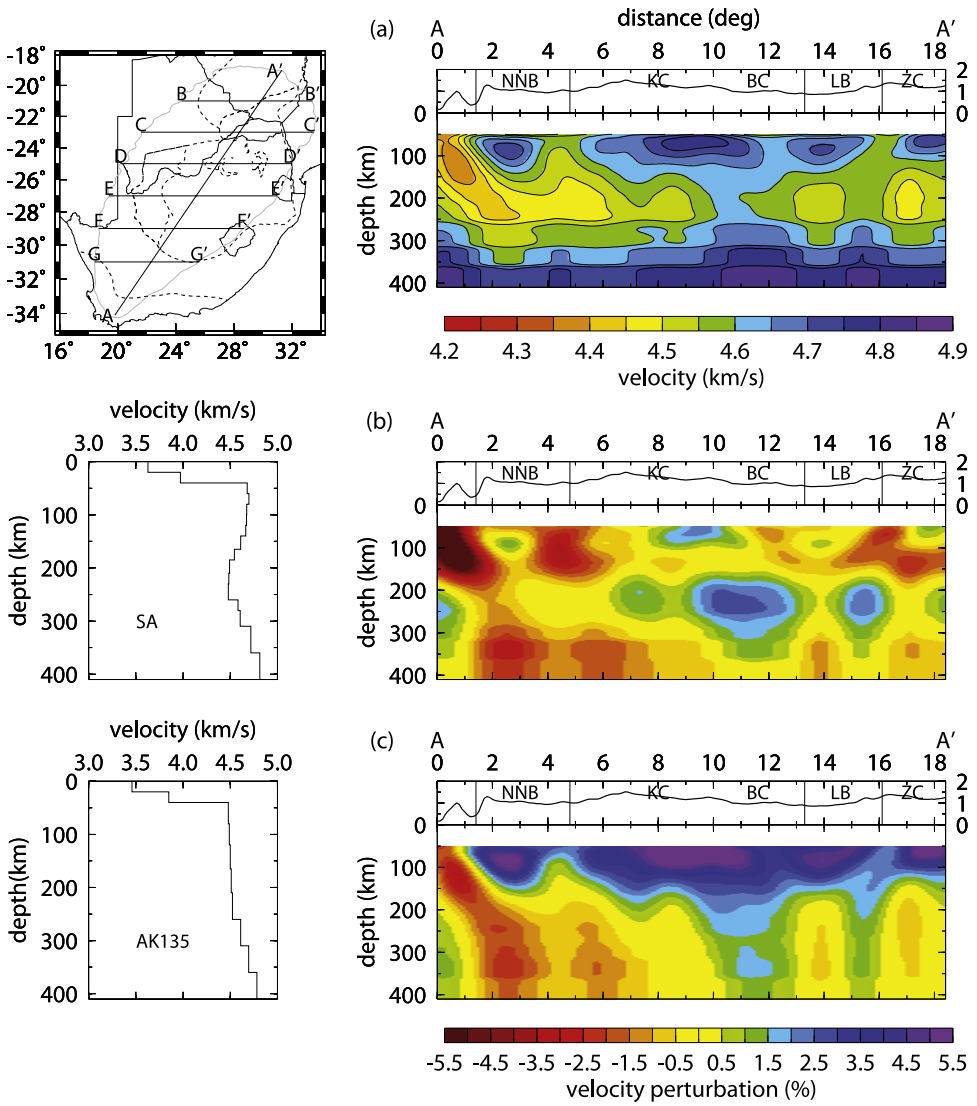

Figure 14. Absolute velocity and velocity perturbation profiles across southern Africa. (a) Velocity profile of A-A′, oriented along the long axis of the array in the SW-NE direction. The location of A-A′ is shown in the map on the left. (b) Velocity perturbation profile of A-A′ relative to the average shear wave velocity in southern Africa (shown on left). (c) Velocity perturbation profile of A-A′ relative to model AK135 (shown on left). Topography is plotted above the velocity and velocity perturbation profiles. Vertical lines in the topography frame indicate tectonic boundaries, and the capital letters represent tectonic provinces as defined in Figure 1.

evidence for craton destruction includes: (1) the removal of the cratonic root under the eastern Sino-Korean craton due to the subduction of the Pacific plate [*Griffin et al.*, 1998; *Gao et al.*, 2004] and (2) a significant low-velocity layer under the Tanzanian craton where rifting is taking place [*Weeraratne et al.*, 2003]. As one of the oldest continental blocks on Earth, the Kaapvaal craton has survived a broad range of destructive events. For instance, the massive outpouring of Karoo basalts [*Duncan et al.*, 1997] and the wide distribution of kimberlites at different ages [*Jelsma et al.*, 2004] all indicate that the southern Africa continent has been disturbed frequently by tectonic activities.

[31] Although different models agree that lithosphere beneath the craton is fast and thick, how deep the Kaapvaal cratonic lithosphere extends remains controversial [*Qiu et al.*, 1996; *Priestley*, 1999; *Zhao et al.*, 1999; *Ritsema and van Heijst*, 2000; *James et al.*, 2001; *Fouch et al.*, 2004]. In this study, we estimated the keel depth on the basis of absolute shear wave velocity variation with depth and found that the keel depth is 180 ± 20 km beneath most parts of the Kaapvaal craton. We used the velocity contours of 4.55 km/s and 4.6 km/s as references for determining the keel depth because they are close to and slightly higher than the shear velocity in a global model at the same depth range. Alternatively, one may determine the keel depth using the medial depth of the low-velocity zone beneath the keel, which would give similar results. The presence of such a LVZ confines the maximum keel depth to 260 km, the base of the LVZ. Another method of defining the keel depth is based on the maximum negative velocity gradient with

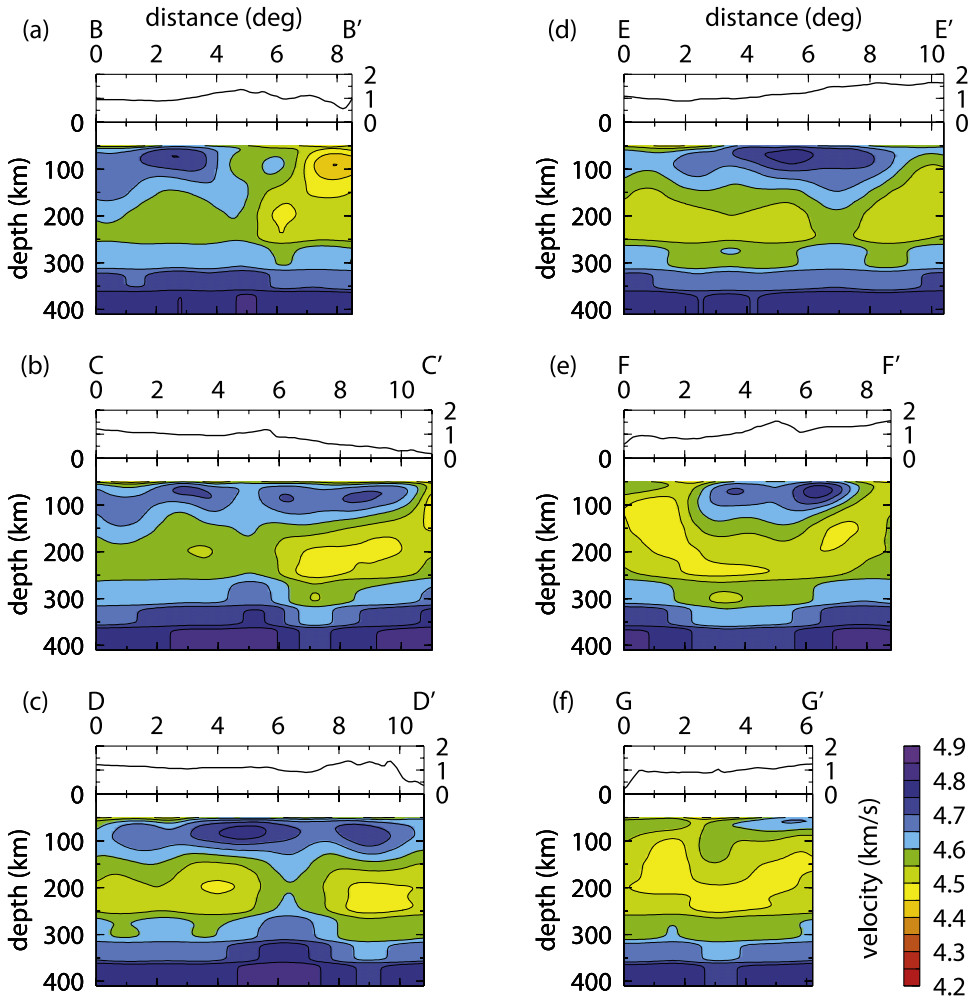

Figure 15. (a–f) Six shear wave velocity profiles in the east-west direction at the depths of 50–410 km. The locations of the profiles are shown on the top left in Figure 14. Topography is plotted above the velocity profiles. A relative low-velocity zone appears on all profiles. Note the good correlation between the topography and the thickness of the low-velocity zone on profile D-D′.

depth [*van der Lee*, 2002]. We calculated vertical velocity gradients for the SW-NE profile but found that the contours of the most negative gradient are very complex and do not match the fast mantle lithosphere imaged in the velocity profile (Figure 14a).

[32] The keel depth obtained from absolute shear wave velocity variation is shallower than that estimated on the basis of high-velocity anomalies. For instance, the maximum keel depth of the Kaapvaal craton is ~210 km on the basis of shear wave velocity variations while fast anomalies under the central craton extend to over 300 km (Figures 14a–14c). Such a thick keel would not make sense because a low-velocity layer would be included in it. Since it is the velocity, not its perturbation, that is directly associated with the physical status of mantle rocks, we believe it is more appropriate to use velocity variation to estimate the keel depth. This finding can explain the difference of the Kaapvaal keel depth between our estimation and others based on velocity perturbation models [*Ritsema and van Heijst*, 2000; *James et al.*, 2001; *Fouch et al.*, 2004], which tend to give a relative thicker keel.

[33] Our estimation of 180 ± 20 km for the keel depth is consistent with a 175–220 km lithospheric thermal thickness derived from heat flow data in southern Africa [*Artemieva and Mooney*, 2001]. The relatively thin root of the Kaapvaal craton is also predicted from the geotherms on the basis of different thermobarometers [*James et al.*, 2004] of mantle xenoliths. The 1300°C adiabat is reached at ~170 km depth on the BK geotherm [*Brey and Kohler*, 1990] and at ~220 km depth on the OW/MC geotherm [*O'Neill and Wood*, 1979; *MacGregor*, 1974]. Although *Rudnick and Nyblade* [1999] constrained the thickness of the Kaapvaal lithosphere at 200–250 km from cratonic xenoliths, a recent xenolith study prefers a thinner chemical boundary layer (~175 km) for cratons [*Lee et al.*, 2005]. Furthermore, the high-temperature peridotites included in the analyses of *Rudnick and Nyblade* [1999] were found to have low seismic velocities [*James et al.*, 2004] and should not be considered as typical, fast cratonic lithosphere.

[34] A relatively fast upper mantle at the depths of 260 to 400 km is observed on the 1-D velocity profile under the northern Kaapvaal craton (Figure 11e) in the Bushveld Complex area. This observation is confirmed in the 3-D

model with much more details. High velocities in the central and northern Kaapvaal craton are imaged continuously to 410 km depth and form a dumbbell shape in the upper mantle (Figures 14a, 15c, and 15d). This dumbbell shape of high velocity resembles mantle downwelling flow in convection models. The relatively high velocity below 260 km in the central and northern Kaapvaal could be the eroded cratonic lithosphere. If so, it can explain a weak but flat 410-km discontinuity observed in the same area [*Gao et al.*, 2002; *Niu et al.*, 2004]. The weakness of the discontinuity could be due to the small velocity contrast across the 410 km because of the relatively fast velocity above it, and the flatness could be interpreted as the opposite effects of high Mg# and cold temperature on the topography of the 410-km discontinuity [*Weidner and Wang*, 2000].

7.2. Low-Velocity Zone in the Southern Africa Upper Mantle

[35] Whether a low-velocity zone exists in the upper mantle of southern Africa has been debated for the past decade. The disagreement in the existing models of southern Africa includes the presence of an LVZ and the variation of its strength and depth [*Nyblade et al.*, 1996; *Qiu et al.*, 1996; *Priestley*, 1999; *Zhao et al.*, 1999; *Simon et al.*, 2002; *Freybourger et al.*, 2001; *Saltzer*, 2002; *Larson*, 2004; *Wang et al.*, 2005]. Our new, high-resolution, shear wave velocity model clearly reveals a reduced velocity layer at the depths of 160–260 km beneath southern Africa. We recognize that velocity in this layer is not absolutely low relative to a global reference model, but is significantly lower than the fast mantle above it.

[36] The LVZ beneath southern Africa cannot be observed on velocity perturbation profiles regardless of a reference model (Figures 14b and 14c). It is therefore not surprising that an LVZ is not revealed in the *P* and *S* wave tomography models in southern Africa [*James et al.*, 2001; *Fouch et al.*, 2004], because those are models of velocity perturbation, not absolute velocities. Similarly, the LVZ is invisible in the velocity perturbation model presented by *Ritsema and van Heijst* [2000]. *Larson* [2004] found that the presence of a weak LVZ depends on an initial model by applying a two-station method to Rayleigh wave data in the southern Kaapvaal craton. We suspect that the sensitivity of *Larson*'s [2004] model to a starting model is due to the lack of constraints from the data and/or too much damping in the model parameters. With much more data and higher resolution in this study, we have found that the LVZ under southern Africa is required by the data and is independent of an initial model.

[37] One problem with the LVZ in southern Africa is the effect of anisotropy. *Saltzer* [2002] pointed out that an artificial low-velocity layer could be imaged when inverting Rayleigh and Love data together for an isotropic model. This may explain the strong LVZ imaged in the model of *Qiu et al.* [1996] where both Rayleigh and Love waveforms were modeled. The artificial effect is not a problem if only one type of surface wave data is used, as in the study of *Priestley* [1999] and in this study. In both studies only Rayleigh wave data were used and the LVZ is much weaker than in the model of *Qiu et al.* [1996].The effect of azimuthal anisotropy on the LVZ is not significant because it must be averaged out given the high density of crossing raypaths. In addition, azimuthal anisotropy is largely confined in the lithosphere of southern Africa and the delay times in the Kaapvaal craton are overall small [*Silver et al.*, 2001, 2004]. Nevertheless, Rayleigh waves are sensitive to Sv structure and a low Sv layer might result from radial anisotropy if $V_{Sv} < V_{Sh}$. However, radial anisotropy has been found to decrease with depth and not to be resolvable below 150 km by *Freybourger et al.* [2001] and *Saltzer* [2002]. We therefore do not think that the observed low-velocity layer in our model can be fully attributed to radial anisotropy although its slowness might be overestimated if such anisotropy exists. Future study combining Rayleigh and Love wave tomography would help to resolve this problem.

[38] A velocity reduction zone in the upper mantle has also been observed beneath other cratons, such as the western Australian craton [*Simons et al.*, 1999], the North American craton [*Grand and Helmberger*, 1984], and the Tanzanian craton [*Weeraratne et al.*, 2003]. On one hand, such a velocity reduction is a common feature of the cratons; on the other hand, the degree of velocity reduction varies significantly beneath different cratons, reflecting the uniqueness of each craton. For example, the lowest velocity in the velocity reduction zone at the depths around 200 km is 4.58 km/s for west Australia, 4.48 km/s for southern Africa, and 4.28 km/s for the Tanzanian craton, respectively (Figure 10) while the velocities in the fast lids are much more consistent among these cratons. The common velocity reduction of shear wave in the upper mantle of cratons can be explained by the decrease of Mg# from the chemical boundary layer above 175 km to the thermal boundary layer beneath it [*Lee et al.*, 2005]. The largest Mg# difference from a fertile mantle (88–89) to a cratonic mantle (92–93) is about 5 units, which only accounts for a shear wave velocity reduction of 1–1.5% based on the Vs-Mg# relation given by *Lee* [2003]. It is clear that the change of Mg# alone cannot explain the large velocity drop of 4% in the LVZ in the upper mantle of southern Africa.

[39] Low shear wave velocity can arise from the effects of petrology, volatiles, and high temperature besides the increase of iron content. *James et al.* [2004] observed a slight (<1%) shear wave velocity reduction with depth in the low-temperature xenoliths in the Kaapvaal craton. Such a petrologic effect is not observed at depths below 170 km and should not be a candidate for the LVZ imaged in the Rayleigh wave model. Even if this effect is applied at the LVZ depth, the resultant velocity reduction would be too small (~1%) to explain our observations (~4%). Volatiles would effectively lower seismic velocities if present. However, the Archaean continents are believed dry to 250 km depth in general [*Hirth et al.*, 2000]. In southern Africa, there is no indication for high volatile content from xenolith data. We therefore do not consider volatiles as candidates for the LVZ beneath southern Africa.

[40] High temperature is probably the dominant mechanism of the LVZ in the upper mantle of southern Africa. The significant velocity reduction from 180 km to 200 km in our Rayleigh wave model (Figure 10) agrees remarkably the shear wave velocities measured from high-temperature lherzolites in the Kaapvaal craton [*James et al.*, 2004], indicating that thermal anomalies that produced those xenoliths are still present in the upper mantle of southern

Africa. In addition, the deformed peridotite xenoliths in the Kaapvaal craton have the largest number and the highest temperature compared with the Slave, Siberia, and Superior cratons [*Rudnick and Nyblade*, 1999], suggesting an anomalous hot upper mantle beneath the Kaapvaal cratonic lithosphere. The LVZ at the depths of 160–260 km beneath the Kaapvaal craton would belong to the thermal boundary layer of the craton [*Lee et al.*, 2005] and is probably subject to mantle convection. The sublithospheric convection in southern Africa could be of the kinds produced in numerical models, such as the plate-wide shallow convection model [*England and Houseman*, 1984; *Burke*, 1996] and the edge-driven convection model [*King and Ritsema*, 2000].

[41] The thermal origin of the LVZ is in accordance with tectonics in southern Africa. Africa is the continent that has experienced the most vigorous hot spot events from the Karoo plume at 90–183 Ma [*Duncan et al.*, 1997; *Morgan*, 1983] to the Afar plume at 31 Ma to the present time [*Burke et al.*, 2003; *Jelsma et al.*, 2004]. These hot spot events frequently provide heating to the upper mantle of Africa. The 2% velocity variation in the LVZ, if purely thermal, could be associated with ~220°C temperature change from the center of the Kaapvaal craton to its edges, which would yield density variations within the LVZ and make contributions to local isostasy. It is difficult to quantify this contribution by correlating the LVZ with the surface topography because of the dominant role of crustal thickness in maintaining local isostasy. In addition, the crustal thickness varies significantly in southern Africa and does not correlate with the topography [*Nguuri et al.*, 2001; *Nair et al.*, 2006]. A more quantitative analysis on isostatic balance in southern Africa could be another research, which is beyond the scope of this paper. In fact, previous studies have shown that surface relief in southern Africa is undercompensated by crustal structure at many SASE stations [*Webb et al.*, 2004] and cannot be completely attributed to dynamic topography associated with low velocities in the lower mantle [*Lithgow-Bertelloni and Silver*, 1998]. Temperature variations in the shallow upper mantle therefore must play an important role in supporting the high topography in southern Africa.

8. Conclusions

[42] A high-resolution, 3-D shear wave velocity model in southern Africa has been constructed from Rayleigh waves at the SASE stations. This model provides new insights into the structure of the cratonic lithosphere and sublithospheric mantle. A fast mantle lithosphere is observed beneath most of southern Africa with thickness varying from ~80 km in the Namaqua-Natal mobile belt to 180–200 km beneath the central and northern Kaapvaal craton. Shear wave velocities beneath the Bushveld Complex are relatively low in the shallow part of the Kaapvaal lithosphere, reflecting the effect of the Bushveld intrusion at ~2.05 Ga. The thickness of the Kaapvaal cratonic keel is estimated at the depths of 180 ± 20 km on the basis of shear wave velocity variation with depth. We imaged a reduced velocity layer at the depths of 160–260 km across southern Africa with variable strength. The increase of iron content below 180 km could account for ~1% shear wave velocity reduction in the cratonic upper mantle and provides a reasonable explanation for a common feature of a weak LVZ in the upper mantle of cratons. However, the observed LVZ in southern Africa is ~4% slower than the keel above, which cannot be fully explained by the decrease of Mg# with depth or other mechanisms, such as volatiles or petrologic effects in the Kaapvaal cratonic lithosphere. We prefer to explain the LVZ in southern Africa by a dominant cause of thermal anomalies, which are associated with sublithospheric convection in the upper mantle. The low-velocity layer is therefore less dense and helps in compensating the high relief in southern Africa.

[43] **Acknowledgments.** We thank the seismic group of the Kaapvaal Project for collecting the data and the IRIS Data Management Center for making the data available to us. Special thanks are given to Matt Fouch for stimulating discussions and constructive comments that helped to improve this manuscript. We thank Dayanthie Weeraratne for providing Rayleigh wave phase velocity data for the Tanzanian craton and some inversion codes. Discussions with Don Forsyth and David James have been helpful. The manuscript has been improved by comments from Karen Fischer and four anonymous reviewers. This work is supported by University of Houston and NSF grants EAR-0125685 and EAR-0338430.

References

Artemieva, I. M., and W. D. Mooney (2001), Thermal thickness and evolution of Precambrian lithosphere: A global study, *J. Geophys. Res.*, *106*, 16,387–16,414.

Brey, G. P., and T. Kohler (1990), Geothermobarometry in four-phase lherzolites. II: New thermobarometers and practical assessment of existing thermobarometers, *J. Petrol.*, *31*, 1353–1378.

Burke, K. (1996), The African plate, *S. Afr. J. Geol.*, *99*, 339–410.

Burke, K., D. S. MacGregor, and N. R. Cameron (2003), Africa's petroleum systems: Four tectonic "aces" in the past 600 million years, in *Petroleum Geology of Africa: New Themes and Developing Technologies*, edited by T. J. Arthur, D. S. MacGregor, and N. R. Cameron, *Geol. Soc. Spec. Publ.*, *207*, 21–60.

Carlson, R. W., T. L. Grove, M. J. de Wit, and J. J. Gurney (1996), Anatomy of an Archean craton: A program for interdisciplinary studies of the Kaapvaal craton, southern Africa, *Eos Trans. AGU*, *77*, 273–277.

Crough, S. T., W. J. Morgan, and R. B. Hargraves (1980), Kimberlites: Their relation to mantle hotspots, *Earth Planet. Sci. Lett.*, *50*, 260–274.

de Wit, M. J., et al. (1992), Formation of an Archean continent, *Nature*, *357*, 553–562.

Duncan, R. A., P. R. Hooper, J. Rehacek, J. S. Marsh, and A. R. Duncan (1997), The timing and duration of the Karoo igneous event, southern Gondwana, *J. Geophys. Res.*, *102*, 18,127–18,138.

Ekstrom, G., J. Tromp, and E. W. Larson (1997), Measurements and global models of surface wave propagation, *J. Geophys. Res.*, *102*, 8137–8157.

England, P., and G. Houseman (1984), On the geodynamic setting of kimberlite genesis, *Earth Planet. Sci. Lett.*, *67*, 109–122.

Forsyth, D. W., and A. Li (2005), Array-analysis of two-dimensional variations in surface wave phase velocity and azimuthal anisotropy in the presence of multipathing interference, in *Seismic Earth: Array Analysis of Broadband Seismograms*, *Geophys. Monogr. Ser.*, vol. 157, edited by A. Levander and G. Nolet, pp. 81–98, AGU, Washington, D. C.

Fouch, M. J., D. E. James, J. C. VanDecar, S. van der Lee, and Kaapvaal Seismic Group (2004), Mantle seismic structure beneath the Kaapvaal and Zimbabwe cratons, *S. Afr. J. Geol.*, *107*, 33–44.

Freybourger, M., J. B. Gaherty, T. H. Jordan, and the Kaapvaal Seismic Group (2001), Structure of the Kaapvaal craton from surface waves, *Geophys. Res. Lett.*, *28*, 2489–2492.

Gao, S. S., P. G. Silver, K. H. Liu, and the Kaapvaal Seismic Group (2002), Mantle discontinuities beneath southern Africa, *Geophys. Res. Lett.*, *29*(10), 1491, doi:10.1029/2001GL013834.

Gao, S., R. L. Rudnick, H.-L. Yuan, X.-M. Liu, Y.-S. Liu, W.-L. Xu, W.-L. Ling, J. Ayers, X.-C. Wang, and Q.-H. Wang (2004), Recycling lower continental crust in the North China craton, *Nature*, *432*, 892–897.

Grand, S. P., and D. V. Helmberger (1984), Upper mantle shear structure of North America, *Geophys. J. R. Astron. Soc.*, *76*, 399–438.

Grand, S. P., R. D. van der Hilst, and S. Widiyantoro (1997), Global seismic tomography: A snapshot of convection in the Earth, *GSA Today*, *7*, 1–7.

Griffin, W. L., A. Zhang, S. Y. O'Reilly, and C. G. Ryan (1998), Phanerozoic evolution of the lithosphere beneath the Sino-Korean craton, in *Mantle Dynamics and Plate Interactions in East Asia*, *Geodyn. Ser.*, vol. 27, edited by M. F. J. Flower et al., pp. 107–126, AGU, Washington, D. C.

Hirth, G., R. L. Evans, and A. D. Chave (2000), Comparison of continental and oceanic mantle electrical conductivity: Is the Archean lithosphere dry?, *Geochem. Geophys. Geosyst.*, *1*(12), doi:10.1029/2000GC000048.

James, D. E., M. J. Fouch, J. C. VanDecar, S. van der Lee, and the Kaapvaal Seismic Group (2001), Tectospheric structure beneath southern Africa, *Geophys. Res. Lett.*, *28*, 2485–2488.

James, D. E., F. Niu, and J. Rokosky (2003), Crustal structure of the Kaapvaal Craton and its significance for early crustal evolution, *Lithos*, *71*, 413–429.

James, D. E., F. R. Boyd, D. Schutt, D. R. Bell, and R. W. Carlson (2004), Xenolith constraints on seismic velocities in the upper mantle beneath southern Africa, *Geochem. Geophys. Geosyst.*, *5*, Q01002, doi:10.1029/2003GC000551.

Jelsma, H. A., M. J. de Wit, C. Thiart, P. H. Dirks, G. Viola, I. J. Basson, and E. Anckar (2004), Preferential distribution along transcontinental corridors of kimberlites and related rocks of southern Africa, *S. Afr. J. Geol.*, *107*, 301–324.

Jordan, T. H. (1975), The continental tectosphere, *Rev. Geophys.*, *13*, 1–12.

Jordan, T. H. (1978), Composition and structure of the continental tectosphere, *Nature*, *274*, 544–548.

Jordan, T. H. (1979), Mineralogies, densities, and seismic velocities of garnet lherzolites and their geophysical implications, in *The Mantle Sample: Inclusions in Kimberlites and Other Volcanics, Proceedings of the Second International Kimberlite Conference*, vol. 2, edited by F. R. Boyd and H. O. A. Meyer, pp. 1–14, AGU, Washington, D. C.

Jordan, T. H. (1988), Structure and formation of the continental tectosphere, *J. Petrol.*, Special Lithosphere Issue. 11–37.

Kennett, B. L. N., E. R. Engdahl, and R. Buland (1995), Constraints on seismic velocities in the Earth from travel times, *Geophys. J. Int.*, *122*, 108–124.

King, S. D., and J. Ritsema (2000), African hot spot volcanism: Small-scale convection in the upper mantle beneath cratons, *Science*, *290*, 1137–1140.

Larson, A. M. (2004), *S*-wave velocity structure beneath the Kaapvaal craton from surface-wave inversions compared with estimates from mantle xenoliths, M.S. thesis, Va. Polytech. Inst. and State Univ., Blacksburg.

Lee, C. T. (2003), Compositional variation of density and seismic velocities in natural peridotites at STP conditions: Implications for seismic imaging of compositional heterogeneities in the upper mantle, *J. Geophys. Res.*, *108*(B9), 2441, doi:10.1029/2003JB002413.

Lee, C. T., A. Lenardic, C. M. Cooper, F. Niu, and A. Levander (2005), The role of chemical boundary layers in regulating the thickness of continental and oceanic thermal boundary layers, *Earth Planet. Sci. Lett.*, *230*, 379–395.

Li, A., D. W. Forsyth, and K. M. Fischer (2003), Shear velocity structure and azimuthal anisotropy beneath eastern North America from Rayleigh wave inversion, *J. Geophys. Res.*, *108*(B8), 2362, doi:10.1029/2002JB002259.

Lithgow-Bertelloni, C., and P. G. Silver (1998), Dynamic topography, plate driving forces, and the African superswell, *Nature*, *395*, 269–272.

MacGregor, I. D. (1974), The system MgO-Al_2O_3-SiO_2: Solubility of Al_2O_3 in enstatite for spinel and garnet peridotite compositions, *Am. Mineral.*, *59*, 110–119.

Morgan, W. J. (1983), Hotspot tracks and the early rifting of the Atlantic, *Tectonophysics*, *94*, 123–139.

Nair, S. K., S. S. Gao, K. H. Liu, and P. G. Silver (2006), Southern Africa crustal evolution and composition: Constraints from receiver function studies, *J. Geophys. Res.*, *111*, B02304, doi:10.1029/2005JB003802.

Nguuri, T., J. Gore, D. E. James, S. J. Webb, C. Wright, T. G. Zengeni, O. Gwavava, J. A. Snoke, and the Kaapvaal Seismic Group (2001), Crustal structure beneath southern Africa and its implications for the formation and evolution of the Kaapvaal and Zimbabwe cratons, *Geophys. Res. Lett.*, *28*, 2501–2504.

Ni, S., E. Tan, M. Gurnis, and D. Helmberger (2002), Sharp sides to the African superplume, *Science*, *296*, 1850–1852.

Niu, F., et al. (2004), Seismic constraints on the depth and composition of the mantle keel beneath the Kaapvaal craton, *Earth Planet. Sci. Lett.*, *224*, 337–346.

Nyblade, A. A., and S. W. Robinson (1994), The African superswell, *Geophys. Res. Lett.*, *21*, 765–768.

Nyblade, A. A., K. S. Vogfjord, and C. A. Langston (1996), *P* wave velocity of Proterozoic upper mantle beneath central and southern Africa, *J. Geophys. Res.*, *101*, 11,159–11,171.

O'Neill, H. S. C., and B. J. Wood (1979), An experimental study of Fe-Mg partitioning between garnet and olivine and its calibration as a geothermometer, *Contrib. Mineral. Petrol.*, *70*, 59–70.

Priestley, K. (1999), Velocity structure of the continental upper mantle: Evidence from southern Africa, *Lithos*, *48*, 45–56.

Qiu, X., K. Priestley, and D. McKenzie (1996), Average lithospheric structure of southern Africa, *Geophys. J. Int.*, *127*, 563–587.

Ritsema, J., and H. van Heijst (2000), New seismic model of the upper mantle beneath Africa, *Geology*, *28*, 63–66.

Ritsema, J., S. Ni, D. V. Helmberger, and H. P. Crotwell (1998), Evidence for strong shear velocity reductions and velocity gradients in the lower mantle beneath Africa, *Geophys. Res. Lett.*, *25*, 4245–4248.

Rudnick, R. L., and A. A. Nyblade (1999), The thickness and heat production of Archean lithosphere: Constraints from xenolith thermobarometry and surface heat flow, in *Mantle Petrology: Field Observations and High Pressure Experimentation: A Tribute to Francis R. (Joe) Boyd*, edited by Y. Fei, C. M. Bertka, and B. O. Mysen, *Spec. Publ. Geochem. Soc.*, *6*, 3–12.

Saito, M. (1988), DISPER80: A subroutine package for the calculation of seismic normal-mode solutions, in *Seismological Algorithms: Computational Methods and Computer Programs*, edited by D. J. Doornbos, pp. 293–319, Elsevier, New York.

Saltzer, R. L. (2002), Upper mantle structure of the Kaapvaal craton from surface wave analysis: A second look, *Geophys. Res. Lett.*, *29*(6), 1093, doi:10.1029/2001GL013702.

Shen, Y., and J. Blum (2003), Seismic evidence for accumulated oceanic crust above the 660-km discontinuity beneath southern Africa, *Geophys. Res. Lett.*, *30*(18), 1925, doi:10.1029/2003GL017991.

Silver, P. G., S. S. Gao, K. H. Liu, and the Kaapvaal Seismic Group (2001), Mantle deformation beneath southern Africa, *Geophys. Res. Lett.*, *28*, 2493–2496.

Silver, P. G., M. J. Fouch, S. S. Gao, and M. Schmitz (2004), Seismic anisotropy, mantle fabric, and the magmatic evolution of Precambrian southern Africa, *S. Afr. J. Geol.*, *107*, 45–58.

Simon, R. E., C. Wright, E. M. Kgaswane, and M. T. O. Kwadiba (2002), The *P* wavespeed structure below and around the Kaapvaal craton to depths of 800 km from traveltimes and waveforms of local and regional earthquakes and mining-induced tremors, *Geophys. J. Int.*, *151*, 132–145.

Simons, F. J., A. Zielhuis, and R. D. Hilst (1999), The deep structure of the Australian continent from surface wave tomography, *Lithos*, *48*, 17–43.

Stankiewicz, J., S. Chevrot, R. D. van der Hilst, and M. J. de Wit (2002), Crustal thickness, discontinuity depth, and upper mantle structure beneath southern Africa: Constraints from body wave conversions, *Phys. Earth Planet. Inter.*, *130*, 235–251.

van der Lee, S. (2002), High-resolution estimates of lithospheric thickness from Missouri to Massachusetts, USA, *Earth Planet. Sci. Lett.*, *203*, 15–23.

Vinnik, L. P., R. W. E. Green, L. O. Nicolaysen, G. L. Kosarev, and N. V. Petersen (1996), Deep seismic structure of the Kaapvaal craton, *Tectonophysics*, *262*, 67–75.

Wang, Y., L. X. Wen, and D. J. Weidner (2005), Upper mantle shear and compressional velocity structures beneath southern Africa, *Eos Trans. AGU*, *86*(52), Fall Meet. Suppl., Abstract S51E-1068.

Webb, S. J., R. G. Cawthorn, T. Nguuri, and D. James (2004), Gravity modeling of Bushveld Complex connectivity supported by Southern African Seismic Experiment results, *S. Afr. J. Geol.*, *107*, 207–218.

Weeraratne, D. S., D. W. Forsyth, K. M. Fischer, and A. A. Nyblade (2003), Evidence for an upper mantle plume beneath the Tanzanian craton from Rayleigh wave tomography, *J. Geophys. Res.*, *108*(B9), 2427, doi:10.1029/2002JB002273.

Weidner, D. J., and Y. Wang (2000), Phase transformation: Implications for mantle structure, in *Earth's Deep Interior: Mineral Physics and Tomography From the Atomic to the Global Scale*, *Geophys. Monogr. Ser.*, vol. 117, edited by S. Karato et al., pp. 215–235, AGU, Washington, D. C.

Yang, Y., and D. W. Forsyth (2006), Regional tomographic inversion of the amplitude and phase of Rayleigh waves with 2-D sensitivity kernels, *Geophys. J. Int.*, *166*, 1148–1160.

Zhao, M., C. A. Langston, A. A. Nyblade, and T. J. Owens (1999), Upper mantle velocity structure beneath southern Africa from modeling regional seismic data, *J. Geophys. Res.*, *104*, 4783–4794.

K. Burke and A. Li, Department of Geosciences, University of Houston, Houston, TX 77204, USA. (ali2@mail.uh.edu)